Mode Vector Modulation: A review

Ioannis Roudas[1], Jaroslaw Kwapisz[2], and Eric Fink[2]
[1]*Electrical and Computer Engineering, Montana State University, Bozeman, MT 59717, USA*
[2]*Department of Mathematical Sciences, Montana State University, Bozeman, MT 59717, USA*
Tel: (406) 994-5960, Fax: (406) 994-5958, e-mail: ioannis.roudas@montana.edu

2023 23rd International Conference on Transparent Optical Networks (ICTON) | 979-8-3503-0303-2/23/$31.00 ©2023 IEEE | DOI: 10.1109/ICTON59386.2023.10207337

ABSTRACT
The use of multidimensional modulations can significantly reduce the energy consumption of optical networks. In this invited paper, we review the essentials of Mode Vector Modulation (MVM), a family of spatial modulation formats used for transmission over multimode/multicore optical fibers or free space. MVM, like Polarization Shift Keying (PolSK) and Stokes Vector Modulation (SVM), can be combined with direct detection and is thus appropriate for future high-capacity, short-haul optical interconnects. The MVM transceiver design, the analytical evaluation of the performance of the optically-preamplified MVM direct-detection receiver, the optimization of MVM constellations using geometric shaping, and the associated bit-to-symbol mapping are the main topics of this review. We show that, in terms of receiver sensitivity, MVM outperforms traditional single-mode, direct-detection-compliant, digital modulation formats by several dB's, and the SNR gain increases with the number of spatial degrees of freedom.
Keywords: Optical communications, direct detection, modulation.

1. INTRODUCTION

Due to their attractive price and low operating cost, M-ary pulse-amplitude modulation (PAM)/direct-detection optical transceivers are currently the most popular choice for links shorter than 10 km [1]. A major drawback of M-PAM is that its energy consumption scales quadratically with the constellation cardinality M as the corresponding signal space is one-dimensional [2]. The quest for short-haul optical communications systems exhibiting better spectral and energy efficiency than their M-PAM/direct-detection counterparts has led to significant advances in non-coherent receiver designs [3]. An interesting development in this area was the resurgence of interest in the polarimetric receiver [4], [5]. Following a similar renovation path as coherent receivers in the early 2000s, the polarimetric receiver was redesigned using novel optical components, analog-to-digital converters, and digital signal processing to counteract polarization rotations during transmission. It is now called the Stokes-vector receiver. Over the last decade, its variants have been considered either for non-coherent detection of various polarization modulation formats, like Polarization Shift Keying (PolSK) and Stokes Vector Modulation (SVM) [4]-[7], or for self-homodyne detection of quadrature modulations, both for single-mode [5] and multimode transmission [8].

In comparison to PAM, M-ary SVM exhibits superior performance because SVM constellation points occupy a three-dimensional Stokes space. As a result, it can be shown that energy consumption scales linearly with the constellation cardinality M [9].

It is possible to generalize the SVM concept, originally intended for single-mode fibers (SMFs), to transmission over N orthogonal spatial and polarization modes (spatial degrees of freedom (SDOFs)). Then, M constellation points can occupy an N^2-1-dimensional Stokes space and energy consumption scales as $M^{\frac{1}{N-1}}$ [9]. This multimode flavor of SVM is dubbed by the authors *Mode Vector Modulation* (MVM) [9]–[15].

In this invited paper, we review the MVM transceiver design, the analytical evaluation of the performance of the optically-preamplified MVM direct-detection receiver, the optimization of MVM constellations using geometric shaping, and the associated bit-to-symbol mapping. We show that, in terms of receiver sensitivity, MVM outperforms traditional single-mode, direct-detection-compliant, digital modulation formats by several dB's, and the SNR gain increases with the number of spatial degrees of freedom.

2. MVM TRANSCEIVER DESIGN

MVM consists in sending pulses of the same shape but different amplitudes and initial phase shifts simultaneously over all spatial and polarization degrees of freedom. Fig. 1a exemplifies the implementation of MVM in the case of a homogeneous two-core fiber with identical, uncoupled, single-mode cores. In this example, there are four spatial and polarization degrees of freedom. We have two states of polarization per core. We launch simultaneously raised-cosine pulses with different amplitudes and initial phases over all four spatial and polarization degrees of freedom. These parallel pulses represent an MVM symbol. We can visualize an MVM symbol either by sketching its intensity plot across the cores or, more accurately, by graphing the polarization ellipses formed by all possible pairs of electric fields of the EM waves propagating over various SDOFs (Fig. 1b). The number of SDOFS N and the number of symbols M in the alphabet are the two parameters that characterize this modulation format, so we write (N, M)-MVM.

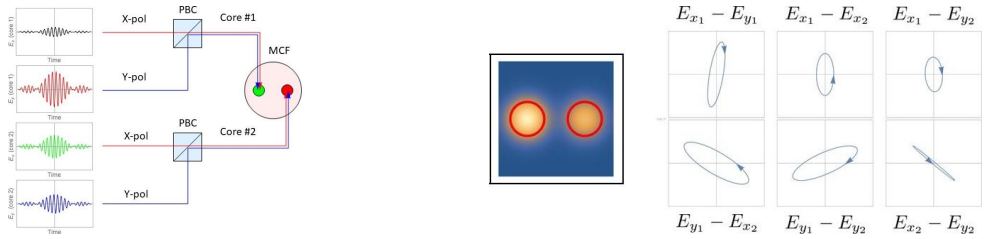

(a) (b)

Figure 1: (a) MVM transmitter implementation and (b) Intensity plot and polarization ellipses representing an MVM symbol propagating over an ideal two-core MCF with identical uncoupled single-mode cores.

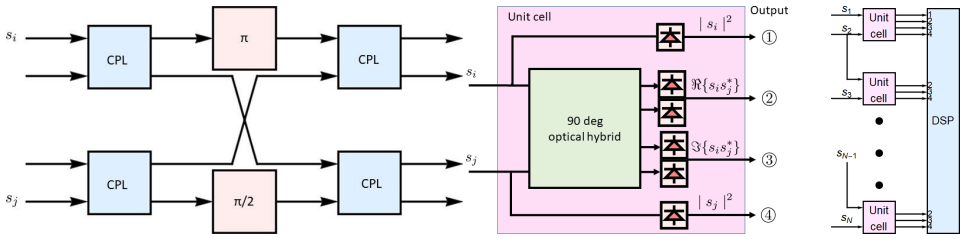

(a) (b) (c)

Figure 2: Mode vector receiver: (a) 90 degree optical hybrid composed of four 3-dB directional couplers and two phase shifters; (b) Unit cell; (c) Cascaded architecture composed of $N-1$ unit cells.

On the receiver side, a 90-degree optical hybrid (Fig. 2a) and four photodiodes can be used to measure the real and imaginary parts of the product $s_i s_j^*$ of two Jones components s_i, s_j of the MVM symbol (Fig. 2b). Two additional photodiodes measure the power of the two components s_i, s_j. Fig. 2b shows a block comprising a 90 degree optical hybrid and six photodiodes. This block be used as a unit cell for MVM receivers. We can concatenate $N-1$ of these unit cells as shown in Fig. 2c. From the measurements performed by the unit cells, the DSP unit can reconstruct the received Stokes vector [13], [14].

3. MVM PERFORMANCE EVALUATION

In this section, we highlight the method for the analytical evaluation of the back-to-back performance of M-ary MVM over N SDOFs in the amplified spontaneous emission (ASE) noise-limited regime. For mathematical tractability, we neglect transceiver imperfections and implementation penalties. These assumptions are justified in the sense that we seek to quantify the ultimate potential of MVM for use in optical interconnects. We model the communication link as an additive white Gaussian noise (AWGN) channel. For equiprobable and equipower signals, the optimal detection scheme based on the *maximum likelihood criterion*, after averaging over all possible random carrier phase shifts is $\hat{m} := \text{argmax}_{1\leq m\leq M} |\langle r|s_m\rangle|$, where $|r\rangle$, $|s\rangle_m$ are the Jones vectors representing the received and candidate symbols, respectively [12], [15].

Fig. 3a shows the decision regions using the above maximum likelihood criterion for 64 equiprobable symbols in the 3D Stokes space $(N=2, M=64)$. To calculate an accurate, closed-form expression for the symbol error probability, one would need to calculate the integral of the tail of the conditional pdf for each transmitted symbol over such irregular boundaries. This can be done potentially only for very small constellations. Unfortunately, the calculation becomes intractable for Stokes spaces of high dimensionality and large constellation cardinalities.

Fig. 3b illustrates the calculation of a tight upper bound on the symbol error probability using the union bound method [2]. For the calculation, we consider all possible pairs of constellation points. Assume that the transmitted symbol is represented by the vector $\hat{s}_m$ in Stokes space and consider the probability of receiving a different symbol $\hat{s}_{m'}$. ASE noise generated at the optical preamplifier can make our received symbol cross the mid-plane that separates $\hat{s}_m$, $\hat{s}_{m'}$. Since the mid-plane represents a much simpler boundary compared to the irregular boundaries shown in Fig. 3a, it is possible to calculate the integral of the tail of the conditional pdf for each transmitted symbol in closed form [12], [15]. The asymptotic expression for the pairwise symbol error probability based on the union bound is $P_{e|s}^{m'|m} \sim \exp\left[-\frac{\gamma_s(1-\gamma)}{2}\right]$, where γ_s is the symbol signal-to-noise ratio (SNR) per SDOF and $\gamma := |\langle s_m|s_{m'}\rangle|$. In the above, $|s_m\rangle$, $|s_{m'}\rangle$ are the Jones vectors corresponding to the Stokes vectors $\hat{s}_m$, $\hat{s}_{m'}$, respectively.

4. MVM CONSTELLATION OPTIMIZATION

4.1 Generalized Thomson problem

In [15], we describe a method to geometrically-optimize constellation points in the generalized Stokes space to optimize the performance of MVM-based links. To facilitate calculations, we do not use the symbol error

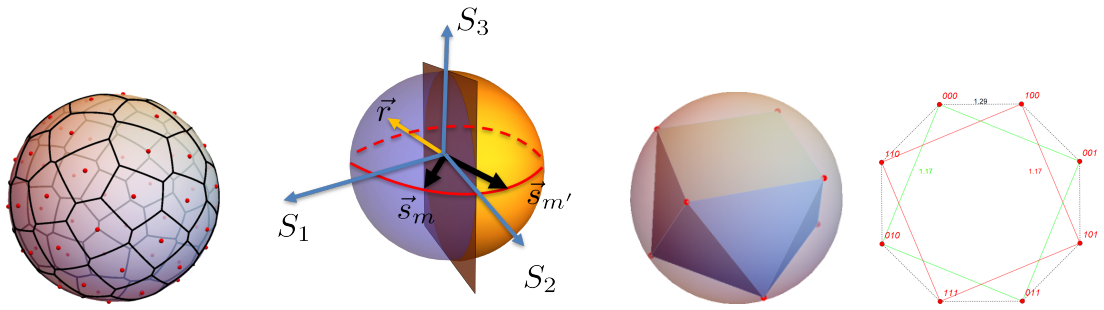

(a) (b) (c) (d)

Figure 3: (a) Voronoi cells for 64 equiprobable symbols (N=2, M=64); (b) Approximate evaluation of the pairwise error probability to decide $\hat{s}_{m'}$ given that $\hat{s}_m$ was transmitted; (c) Square antiprism (Conditions: $N = 2$, $M = 8$); (d) Bit-to-symbol mapping for the square antiprism (Conditions: $N = 2$, $M = 8$). The red, green, and black edges have lengths of approximately 1.17, 1.17, and 1.29, respectively.

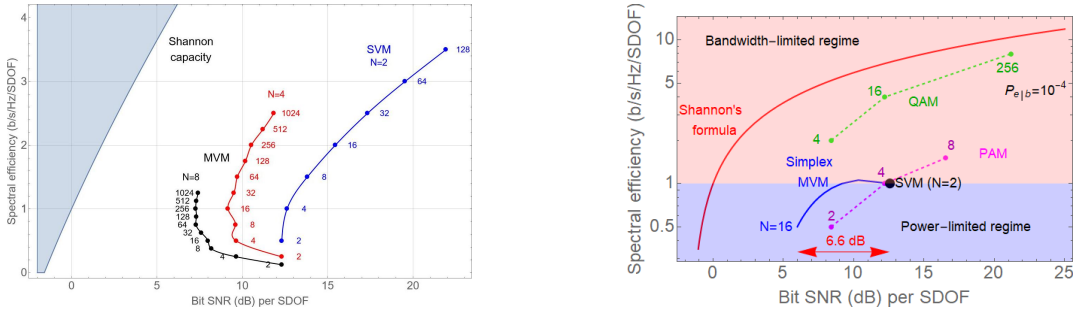

(a) (b)

Figure 4: (a) MVM spectral efficiencies per spatial degree of freedom (SDOF) vs the bit SNR per SDOF required to achieve a bit error probability of 10^{-4} for different degrees of freedom N and constellation cardinalities M. Blue, red, and black curves correspond to $N = 2, 4, 8$, respectively. The number listed next to each point corresponds to the constellation cardinality; (b) Simplex MVM spectral efficiencies per spatial degree of freedom (SDOF) vs the bit SNR per SDOF required to achieve a bit error probability of 10^{-4} (in blue). Results for coherent PAM, QAM, and SVM for various constellation cardinalities are also shown.

probability as an objective function. Instead, we resort to an electrostatic analog where the constellation points are modeled as identical charges free to move on the surface of a conducting Poincaré hypersphere. This approach is a generalization of the Thomson problem: finding the configuration of identical charges on the surface of a conducting 3D sphere such that the total potential energy is minimized. Starting with a random distribution of constellation points on the hypersphere, we use the method of gradient descent to minimize the electrostatic potential.

To test the validity of this approach, we examine the optimal distribution of eight points on the surface of the Poincare sphere S^2. The optimal constellation corresponds to a square antiprism [17] as shown in Fig. 3c. Over numerous trials of different initial configurations, our gradient descent method converges to a final constellation that is approximately identical to the one of Benedetto et al. [17]. While the Euclidean distances between constellation points are slightly different, the differences are immaterial for practical engineering purposes.

4.2 BIT-TO-SYMBOL MAPPING

Once an MVM constellation is geometrically optimized by solving the generalized Thomson problem, it is necessary to optimize the bit-to-symbol mapping to minimize the bit errors. In general, MVM constellations are not amenable to Gray coding. Instead, bits must be mapped to the constellation points using a recursive algorithm. One approach to optimizing the bit-to-symbol mapping is to use simulated annealing to minimize the Hamming distance between the closest neighbors in the constellation [11], [15].

As an example, Fig. 3d shows the optimal bit-to-mapping for the square antiprism provided by simulated annealing. To facilitate visualization, we can represent the configuration of constellation points on the surface of the Poincaré sphere by a two-dimensional graph whose vertices represent the constellation points and its edges represent closest neighbors. The two square faces on opposite sides of the square antiprism are shown in red and green respectively, and the edges interconnecting them are shown with dotted black lines. The proposed bit-to-symbol mapping in Fig. 3d offers almost all the benefits of Gray coding. Each probable symbol error leads to 3 neighboring nodes that differ by one bit and to only one neighboring node that differs by two bits.

5. SPECTRAL EFFICIENCY - ENERGY EFFICIENCY TRADE-OFF

Fig. 4a shows the relationship between the MVM spectral efficiency per SDOF and the bit SNR per SDOF required to achieve a bit error probability of 10^{-4} for different degrees of freedom N and constellation cardinalities M. Each curve in Fig. 4a corresponds to a different value of N, while each point within a curve corresponds to a different value of M. The curves represent geometrically-shaped constellations with optimized bit-to-symbol mapping.We notice that the MVM spectral efficiency η as a function of the bit SNR per SDOF in dB $\gamma_b(dB)$ is a C-shaped curve, with the upper section increasing linearly with $\gamma_b(dB)$ and the lower section decreasing exponentially with $\gamma_b(dB)$. The apex of each C-shaped curve for $N > 2$ occurs for simplex constellations. We conclude that simplex constellations represent the best compromise between spectral and energy efficiencies for $N > 2$.

In Fig. 4b, we compare the performance of simplex MVM to conventional modulation formats with direct- and coherent-detection. The blue curve in Fig. 4b shows the evolution of spectral efficiency per SDOF as a function of the bit SNR per SDOF required to achieve a bit error probability of 10^{-4} for simplex MVM for different degrees of freedom N. In comparison, the red curve represents Shannon's formula for the spectral efficiency of an additive white Gaussian noise (AWGN) channel. The maximum spectral efficiency for simplex MVM is achieved at $N = 3$ and is equal to 1.06 b/s/Hz/SDOF. For $N = 2 - 4$, the spectral efficiency is approximately equal to that of binary intensity modulation per SDOF, which is 1 b/s/Hz/SDOF. As N increases beyond 4, the spectral efficiency decreases. We notice that simplex MVM offers a sensitivity improvement of 6.6 dB for $N = 16$ compared to conventional simplex SVM over SMFs ($N = 2$). This improvement comes at a cost, however, since spectral efficiency per SDOF decreases and receiver hardware complexity increases by increasing the number of SDOFs N. Overall, we conclude that using MVM over N orthogonal SDOFs is beneficial, as it offers greater flexibility for balancing energy consumption and spectral efficiency compared to SVM over two SDOFs.

6. SUMMARY

In this invited paper, we introduced the readers to Mode vector modulation (MVM), a novel approach that extends the concept of Stokes vector modulation (SVM) to few-mode or multicore fibers, as well as free space. MVM enhances the energy efficiency of short-haul optical communications systems by taking advantage of the available spatial degrees of freedom (SDOFs) in the aforementioned media. The spatial degrees of freedom are utilized as one channel, rather than as individual channels, as in the case of space division multiplexing (SDM). In other words, in MVM, a single bit stream is represented by optical pulses transmitted in parallel over multiple spatial and polarization modes. Pulses have the same shape but different amplitudes and initial phases. By jointly optimizing the pulses' amplitudes and phases, MVM can achieve higher spectral efficiency and better energy efficiency compared to conventional modulation schemes that only use the quadratures of a single mode. We showed that the best trade-off between spectral efficiency and energy consumption for $N > 2$ occurs for simplex constellations.

REFERENCES

[1] X. Pang *et al*., *J. Light. Technol.*, vol. 38, pp. 492–503, 2020.
[2] J. G. Proakis and M. Salehi, *Digital Communications*, 5th ed. McGraw-Hill, 2007.
[3] M. Chagnon, *J. Light. Technol.*, vol. 37, no. 8, pp. 1779, 2019.
[4] K. Kikuchi and S. Kawakami, *Opt. Express*, vol. 22, no. 7, pp. 7374, Mar. 2014.
[5] D. Che *et al*., *J. Light. Technol.*, vol. 33, no. 3, pp. 678, 2015.
[6] M. Morsy-Osman *et al*., *J. Light. Technol.*, vol. 34, no. 7, pp. 1585, 2016.
[7] T. Tanemura and Y. Nakano, *IEICE Trans.*, vol. E101.C, no. 7, pp. 594, 2018.
[8] H. Ji *et al*., *Optics Letters*, vol. 44, no. 8, pp. 2065, 2019.
[9] I. Roudas *et al*., OFC 2023, paper no. Th3E.4.
[10] I. Roudas *et al*., ECOC 2021, paper no. Tu2D.5.
[11] E. Fink *et al*., IPC 2021, paper no. TuE3.2.
[12] J. Kwapisz *et al*., CLEO 2022, paper no. SM4J.1.
[13] J. Kwapisz *et al*., IPC 2022, paper no. TuF1.3.
[14] J. Kwapisz *et al*., ACP 2022, pp. 670.
[15] J. Kwapisz *et al*., ArXiv. /abs/2303.09776.
[16] I. Roudas and J. Kwapisz, IEEE Photon. J., vol. 9, no. 5, pp. 1, 2017.
[17] S. Benedetto and P. T. Poggiolini, IEEE Trans. Commun., vol. 42, nos. 2–4, pp. 1174, Feb. 1994.